Application of RADAR Technology to Aerial LIDAR Systems for Enhancement of Shallow Underwater Target Detection

Linda Jeanne Mullen, Amarildo J. C. Vieira, Peter R. Herczfeld, *Fellow, IEEE*, and Vincent Michael Contarino

Abstract—**Since microwaves do not penetrate water, RADAR, the principal tool for remote sensing of the earth and atmosphere, cannot be used directly for the detection of underwater objects. Currently, aerial light detecting and ranging (LIDAR) systems are therefore preferred for the detection and ranging of objects submerged in the sea. LIDAR provides for large area coverage at high speed, but it lacks coherent detection capability, a shortcoming that severely limits system sensitivity and underwater target contrast. In response to this problem, this paper details the merging of RADAR and LIDAR technologies in the constitution of a hybrid LIDAR-RADAR detection scheme. This new sensor configuration has reduced incoherent backscatter clutter by 17 dB in laboratory experiments and related computer simulations.**

I. Background

SINCE the early 1930's, acoustic echo sounders have dominated the field of underwater surveying; however, the slow speed of the transporting surface vessel results in a limited area coverage rate. Since survey ships operate in relatively deep waters, shallow water surveying remains a challenge. Thus, the need for faster, more efficient, and more accurate techniques for shallow underwater surveying has led to the development of airborne light detecting and ranging (LIDAR) systems. The benefits of LIDAR over SONAR include an increase in coverage rate and area and an improved spatial distribution of soundings [1].

The basic aerial LIDAR system consists of an optical transmitter and receiver mounted in an aircraft which flies over the ocean. The optical transmitter is a pulsed frequency-doubled Nd:YAG laser with an output at a wavelength of 532 nm. The blue-green wavelength minimizes absorption in water, while the Nd:YAG laser is favored for its ability to provide short pulses with high peak power, simplicity, ruggedness, and reliability [2]. The collinear optical receiver consists of light-collecting optics, a spatial filter to limit the receiver acceptance angle (or receiver field of view), an optical filter (to suppress background radiation such as stray sunlight), an optical detector, and signal processing apparatus.

Manuscript received January 13, 1995; revised March 19, 1995. This work was supported by the National Science Foundation through the Graduate Engineering Education Fellowship for Women and Minorities at Drexel University, the Brazilian Ministry of Science and Technology, RHAE Program, Grant #111/90, and the Naval Air Warfare Center, Contract #N62269-93-0501.

L. Mullen, A. Vieira, and P. R. Herczfeld are with the Center for Microwave-Lightwave Engineering, Drexel University, Philadelphia, PA 19104 USA.

V. M. Contario is with the Naval Air Warfare Center, Warminster, PA 18974 USA

IEEE Log Number 9413687.

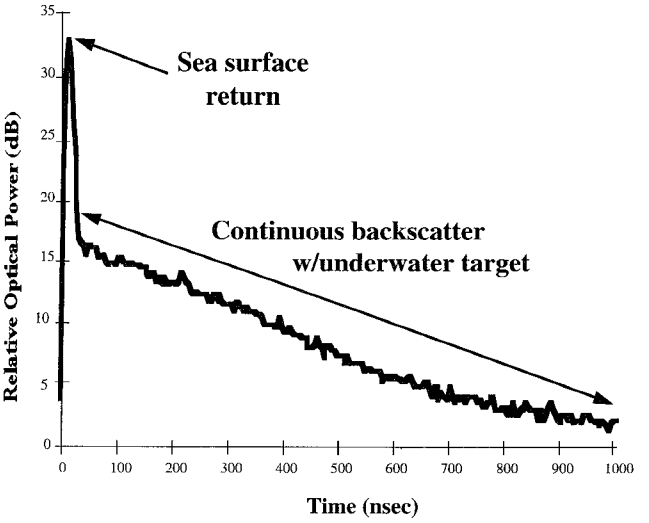

Fig. 1 LIDAR waveform with sea surface return and shallow underwater target reflection hidden by continuous water backscatter.

The transmitted beam sweeps along the water surface with scanning mirrors at an angle, θ, to the vertical. At the air/water interface, the light is both reflected and refracted into the water medium, where it is attenuated due to absorption and scattering as it propagates to the ocean bottom. It is also reflected from underwater objects, the ocean bottom, and randomly backscattered from the ocean mass. The entire return signal is captured by the optical receiver, and analyzed. Finally, the amplitude of the echo signal, which contains the underwater target information, is displayed versus time.

The continuous scattering of the optical beam by entrained particulates in the water introduces dispersion and background clutter, which adversely affects the performance of LIDAR. Scattering causes the initially collimated light beam to disperse spatially into a cone of a continuously increasing angle as it propagates to the ocean bottom and back. The spatial dispersion of the optical beam translates into temporal dispersion of the return signal from an underwater object due to path length differences in the reflected light.

A typical LIDAR echo signal, comprised of the ocean surface reflection, the continuous scattering from the ocean mass, and a reflection from a shallow underwater target, is shown in Fig. 1. This figure also exposes the critical inadequacy of

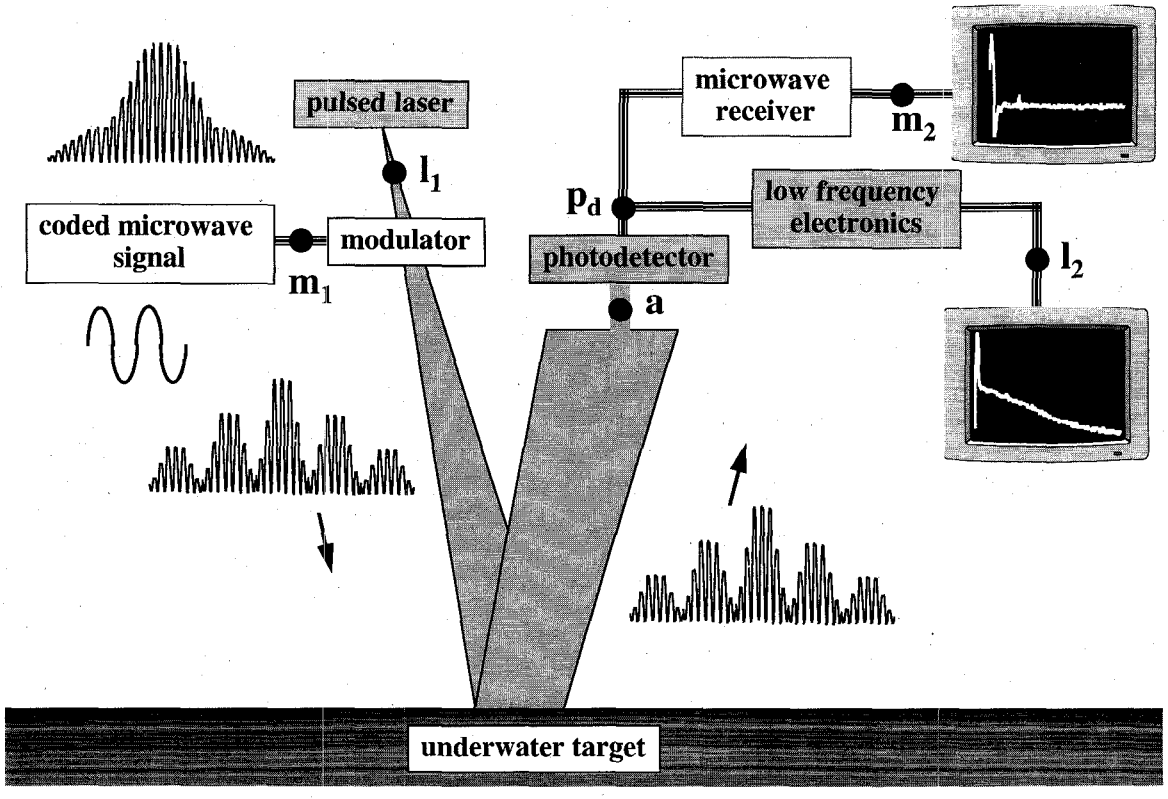

Fig. 2. Block diagram of hybrid LIDAR-RADAR system implementation.

conventional LIDAR. The primary effect of the continuously backscattered light from water is to produce a clutter that limits the contrast of near-surface underwater target reflections and, therefore, decreases the detection sensitivity. Dispersion, while critical in deep water exploration, is of lesser concern in shallow water searches. The principal task, therefore, is to find a method that minimizes this backscatter clutter and thereby improves the detection sensitivity of existing LIDAR systems.

II. Hybrid Lidar-Radar—A Novel Technology

Since the first demonstrations of the ability of radio waves to be reflected by metallic and dielectric bodies by Heinrich Hertz in 1886, the use of RADAR on the ground, in the air, and on the sea to locate remote objects has been extensive [3]. This technology has experienced many advances in its history, one of which involves sophisticated coherent detection schemes. However, the benefits of microwave RADAR cannot be used directly for underwater detection since microwaves do not penetrate water. Techniques based on coherent detection cannot be applied to LIDAR because light rapidly loses coherency as it travels through water.

The solution explored in this paper comprises of the merging of RADAR and aerial LIDAR for the design of a novel hybrid LIDAR-RADAR system, as shown in Fig. 2. Through the combination of the signal processing of microwave RADAR and the underwater transmission capacity of LIDAR, a detection mechanism with superior attributes has been instituted. Referring to Fig. 2, between points l_1 and l_2 we have the basic LIDAR system as it exists today. The laser generates pulsed blue-green optical radiation, which penetrates deep into the water, and the return signal is captured by an optical detector and investigated for the underwater target information. The application of RADAR to the LIDAR system is also depicted in this figure. At point m_1, a microwave envelope is superimposed on the optical carrier by a high-speed modulator. The blue-green optical carrier then transports the microwave signal through the water. The reflected optical signal, with the microwave envelope, is detected by an aerial optical receiver. At point m_2, the microwave signal is recovered by a high-speed photodetector. Therefore, between points m_1 and m_2 we have a RADAR system that can be subjected to well-established coherent signal processing. This approach essentially enables one to transmit a RADAR signal underwater as a subcarrier to render target detection and ranging. At the receiver, both the optical carrier (LIDAR signal) and the microwave envelope (hybrid LIDAR-RADAR signal) can be examined simultaneously from a single measurement.

III. Clutter Suppression By Use of Lidar-Radar

To ascertain how the hybrid LIDAR-RADAR will enhance the detection of underwater targets, we must analyze the system depicted in Fig. 2 in more detail. The unmodulated, conventional LIDAR between points l_1 and l_2 is considered first. With omission of dispersion, the amplitude of the optical signal that enters the detector (at point a) is the sum of the return signal from the ocean surface ($\mathcal{A}_s$), backscatter from the water ($\mathcal{A}_i$), the echo from an underwater target ($\mathcal{A}_t$), and the reflection from the ocean bottom ($\mathcal{A}_b$)

$$\mathcal{A}_T = \mathcal{A}_s + \sum_i \mathcal{A}_i + \mathcal{A}_t + \mathcal{A}_b \tag{1}$$

where

$$\begin{aligned}
\mathcal{A}_s &= \mathcal{A}_{so}e^{-2ar_s} \\
&= \mathbf{a}_{so}e^{-2act_s}e^{j2\pi\nu(t-t_s)} \\
\mathcal{A}_i &= \mathcal{A}_{io}e^{-2ar_s}e^{-2b(r_i-r_s)} \\
&= \mathbf{a}_{io}e^{-2act_s}e^{j2\pi\nu(t-t_i)}e^{-2bv(t_i-t_s)} \\
\mathcal{A}_t &= \mathcal{A}_{to}e^{-2ar_s}e^{-2b(r_t-r_s)} \\
&= \mathbf{a}_{to}e^{-2act_s}e^{j2\pi\nu(t-t_t)}e^{-2bv(t_t-t_s)} \\
\mathcal{A}_b &= \mathcal{A}_{bo}e^{-2ar_s}e^{-2b(r_b-r_s)} \\
&= \mathbf{a}_{bo}e^{-2act_s}e^{j2\pi\nu(t-t_b)}e^{-2bv(t_b-t_s)}.
\end{aligned}$$

In the above expressions, which represents the spatial and temporal response of the LIDAR, r_s, r_i, r_t, and r_b are the positions of the ocean surface, distributed scatterer, target, and ocean bottom. In (1), the propagation velocities and the attenuation coefficients in the air and water are denoted by the symbols c, $v = c/n$, a and b, respectively. The frequency of the optical carrier is ν and the coefficients $\mathcal{A}_{j0}$ and $\mathbf{a}j0$ are constants.

To reduce the complexity of the LIDAR signal, several simplifying assumptions are introduced. First, as is customary in LIDAR studies, we set the time reference at the arrival of the surface return ($t_s = 0$). Secondly, we assume that the underwater object is spatially separated from the ocean surface or ocean bottom by a distance greater than the pulse length, which is in the range of 5–10 feet, so that the receiver can discriminate the return from the ocean surface and bottom. This second assumption enables us to neglect, for the present, $\mathcal{A}_s$ and $\mathcal{A}_b$ so that we can concentrate on the clutter problem.

The output of the optical detector is proportional to the absolute magnitude of the incident optical signal, $I\mathcal{A}_T I^2$. Since the coherence length of the laser in the water is very short the cross terms will vanish, and we may write

$$|\mathcal{A}_T|^2 = \sum_i |\mathcal{A}_i|^2 + |\mathcal{A}_t|^2 \tag{2}$$

where the first term represents the clutter and the second term corresponds to the signal from the target. The contrast problem in LIDAR is related to the fact that the first term dominates the return. The detected LIDAR return, $P_{dL}(t)$ at point p_d, which is proportional to $I\mathcal{A}_T I^2$, can be written as

$$\begin{aligned}
P_{dL}(t) = P(t) \otimes &\left(\frac{\eta F A_r}{R^2}\right) \\
&\cdot \left[\sum_i \rho_i e^{-2\alpha v t_i \delta(t-t_i)} + \rho_t e^{-2\alpha v t_t \delta(t-t_t)}\right]
\end{aligned} \tag{3}$$

where $P(t) = P_o u(t)$ is the transmitted signal with power P_o and $u(t)$ is the step function, η is a term which accounts for the efficiency of the transmitting and receiving optics, F defines the finite field of view, A_r is the effective aperture area of the optical receiver, and $\otimes$ denotes the convolution operator. The square law spreading loss, denoted by R, is considered to be a constant since the airplane altitude is much larger than the depth of the water medium. The reflectivities of the individual scatterers is ρ_i and the reflectivity of the target is ρ_t. The composite power attenuation coefficient in the water due to scattering and absorption is α.

Although the formulation considered here is for continuous wave signals, it can be readily extended for a pulsed source. In addition, the above equation accounts for an inhomogeneous water column by imposing a dependency of the scatterer reflection coefficient on depth. However, this restriction is removed in most LIDAR simulation studies [1], and a uniform reflection coefficient, ρ, is introduced. Since the distribution of particulate matter within the water mass is very dense, in LIDAR studies it is customary to restate (3) in a continuous form [4]

$$\begin{aligned}
P_{dL}(t) &= P(t) \otimes \left(\frac{\eta F A_r}{R^2}\right) \\
&\quad \cdot \{\rho e^{-2\alpha v t}[u(t) - u(t-t_d)] + \rho_t e^{-2\alpha v t_t \delta(t-t_t)}\} \\
&= P(t) \otimes H_{dL}(t) = P(t) \otimes [H_i(t) + H_t(t)]
\end{aligned}$$

where $H_{dL}(t)$ is the impulse response of the water, with a component for backscatter (H_i) and target (H_t). The search time, $t_d = L/v$, relates to the depth of the water column searched, L. The frequency response is obtained by taking the Fourier transform of $H_{dL}(t)$

$$\begin{aligned}
H_{dL}(f) &= H_i(f) + H_t(f) \\
&= \left(\frac{\eta F A_r}{R^2}\right) \\
&\quad \cdot \left[\rho \frac{1 - e^{-2\alpha v t_d} e^{j4\pi f t_d}}{\alpha v - j2\pi f} + \rho_t e^{-2\alpha v t_t} e^{j4\pi f t_t}\right].
\end{aligned} \tag{4}$$

The term corresponding to continuous backscatter from the water mass has a low-pass filterlike response with a corner frequency of $f_c = \alpha v/2\pi$ when $\alpha v t_b > 1$. The expression representing the reflected signal from an underwater target is a phase term which is directly proportional to the target depth. The amplitude frequency response, $|H_{dL}(f)|$, of a typical LIDAR return is illustrated in Fig. 3. We note that while the amplitude of the target reflection, $|H_t(f)|$, remains relatively independent of frequency, the backscatter response, $|H_i(f)|$, decays for frequencies above f_c. Although no explicit information exists for the corner frequency, one can estimate it from tabulated water attenuation data [5] to be in the range of 2–10 MHz, with the lower values for clear water. This range suggests a modulating frequency substantially above the corner frequency, f_c, where the noise due to backscatter is diminished, but target reflections are unaffected.

Let us now consider the hybrid LIDAR-RADAR case in which the RADAR signal, with microwave frequency f_m, is applied to the modulator at point m_1 in Fig. 2. The transmitted optical power, $P_m(t)$, takes the form, $P_m(t) = P_o[1 + m\cos(2\pi f_m t)]\,u(t)$, where m is the modulation index. The detected hybrid LIDAR-RADAR return, $P_{dLR}(t)$, at point p_d is

$$\begin{aligned}
P_{dLR}(t) &= P_m(t) \oslash H_{dL}(t) \\
&= P_{dL}(t) + P(t)m\cos(2\pi f_m t) \oslash H_{dL}(t) \\
&= P_{dL}(t) + P_{dR}(t).
\end{aligned} \tag{5}$$

Thus, the return signal is comprised of the original unmodulated LIDAR echo, $P_{dL}(t)$, and a term corresponding to the

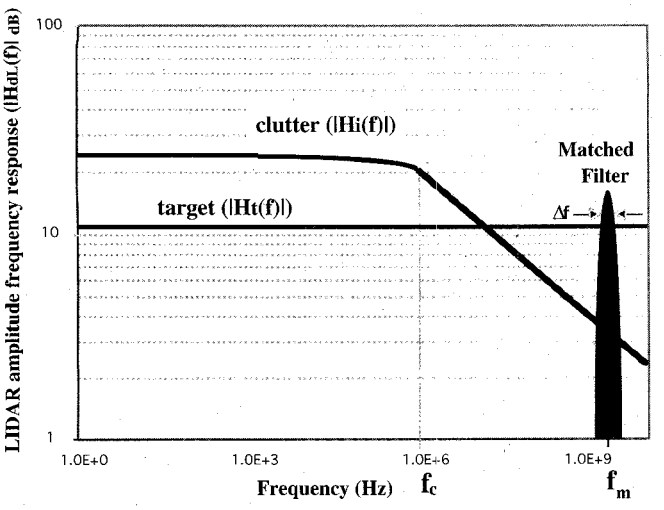

Fig. 3. Amplitude frequency response of LIDAR return signal containing target $[|H_t(f)|]$ and backscatter $[|H_i(f)|]$ components with $C_1 = 10\log(\eta F A_r \rho/\alpha v R^2)$ and $C_2 = 10\log(\eta F A_r \rho_t/R^2) - 20\alpha v t_t$.

interaction of the microwave envelope with the water medium, $P_{dR}(t)$. The convolution in (5) yields the expression for the cw microwave modulated return

$$P_{dR}(t) = P_0 \left\{ \left(\frac{m\eta F A_r}{R^2} \right) \cdot \left[\frac{\sum_j \rho_j \cos(2\pi f_m t + \phi_j) e^{-2\alpha v t_i}}{\alpha v \sqrt{1 + \left(\frac{f}{f_c}\right)^2}} + \rho_t \cos(2\pi f_m t + \phi_t) e^{-2\alpha v t_t} \right] \right\}$$

$$= P_0\{G_i(t) + G_t(t)\}. \quad (6)$$

The phase terms, ϕ_j and ϕ_t, account for the delay of the RADAR signal from its interaction with the particulate matter and the target within the water column. The summation represents the accumulation of microwave envelopes, with random phase delays, emanating from the individual, randomly distributed scatterers. This sum, while not negligible, is small due to the random nature of ϕ_j.

Next we examine and compare the signals at points l_2 and at m_2. The LIDAR signal at l_2 is

$$S_L(t) = P_{dLR}(t) \otimes H_L(t) = P_{dL}(t) \otimes H_L(t) + P_{dR}(t) \otimes H_L(t) \quad (7)$$

where $H_L(t)$ is the transfer function of the low frequency electronics, which filters out the microwave portion of the signal. Therefore, (7) becomes

$$S_L(t) \cong P_{dL}(t) \otimes H_L(t) = \{P(t) \otimes [H_i(t) + H_t(t)]\} \otimes H_L(t).$$

The signal at m_2 is

$$S_M(t) = P_{dLR}(t) \otimes H_M(t) = P_{dL}(t) \otimes H_M(t) + P_{dR}(t) \otimes H_M(t). \quad (8)$$

where H_M is the transfer function of the microwave receiver, consisting of a narrow band-pass filter with center frequency $f_m \gg f_c$, and a microwave detector. The matched filter eliminates the low frequency part of the return yielding

$$S_M(t) \cong P_{dR}(t) \otimes H_M(t) = P_0[G_i(t) + G_t(t)] \otimes H_M(t)$$

For the conventional LIDAR, (7), the return is dominated by the low frequency clutter [characterized by $H_i(t)$], which effectively masks the target reflection. In the RADAR case, the effect of the low-frequency clutter is replaced by the composite backscatter of the microwave envelope, G_i. Since the phases of these high-frequency returns are randomly distributed, their sum will tend to zero. However, the distinct return from the underwater target will retain the coherency of the microwave envelope and will appear unaffected in the return.

To compare the hybrid system and its LIDAR counterpart, (7) and (8) were evaluated for a representative LIDAR experiment using narrow laser pulses. Pulse widths ranging from 5–20 ns are common in LIDAR, which implies a modulation frequency in the GHz range if the pulse is to contain several microwave cycles. A 10 ns pulse modulated at 3 GHz was selected for this computation. The bandwidth of the low-frequency electronics was given the typical value of 100 MHz, while the passband of the matched microwave receiver was variable. The results revealed a target contrast increase from 20–38 dB as the passband of the microwave filter is decreased from 500–3 MHz. Clearly, the hybrid detection scheme has the potential to significantly enhance the detection sensitivity of underwater objects by suppressing incoherent backscatter clutter.

In previous sections, we introduced a new methodology, a hybrid LIDAR-RADAR detection system, which asseverates to reduce the clutter that limits the performance of LIDAR. Next, we turn our attention to proof-of-concept type experimentations to verify this assertion. First, the development of an extensive computer simulation, which enables us to investigate alternate modulation formats and receiver configurations, is discussed. Second, an empirical ocean mass simulator (OMS), which realistically and accurately reproduces the optical properties of the ocean, will be described. The laboratory experiment utilizing the OMS and implementing the hybrid detection scheme is then examined.

IV. LIDAR System Computer Simulation

In parallel with the development of the OMS, a computer simulation was implemented with the aim of reproducing the characteristic signature obtained in the LIDAR system and the OMS. The simulation, with built-in signal processing

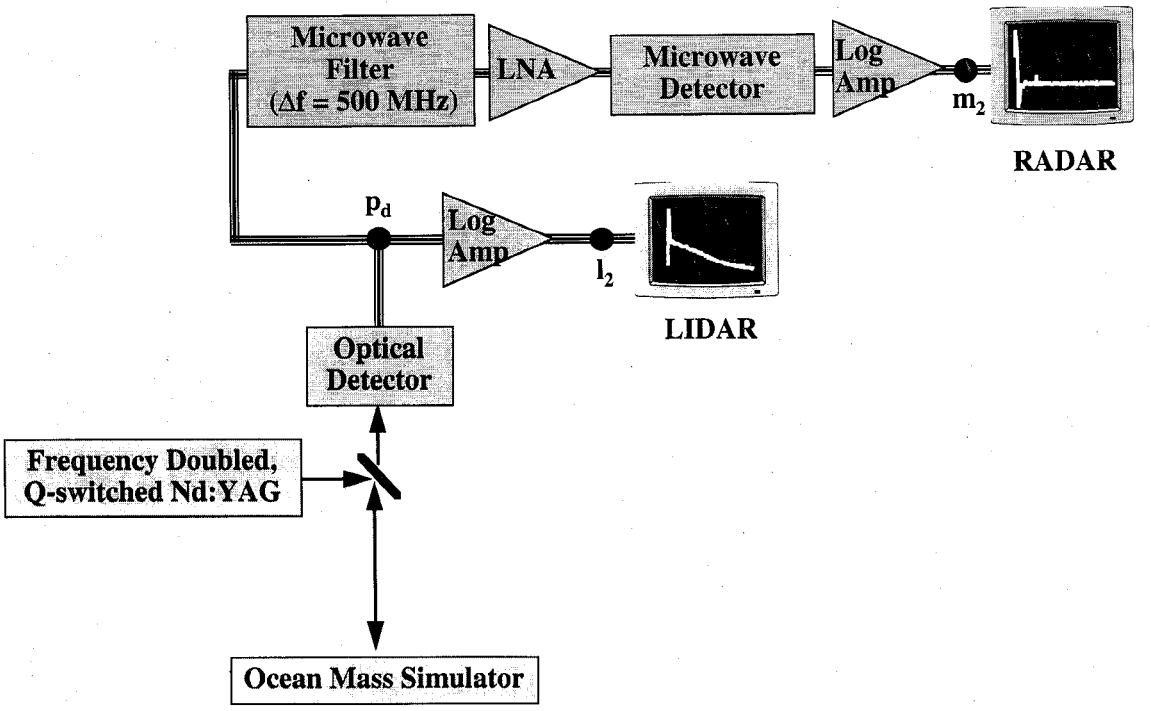

Fig. 4. Laboratory experimental setup with implementation of hybrid LIDAR-RADAR detection scheme.

procedures, predicts laboratory results and helps in the design of more advanced transmitter and receiver configurations.

The simulation is based on (5) [or (7) and (8)], and the pertinent parameters employed in the runs are described below. The length of the water column searched, L, was partitioned into compartments, with length Δl each containing a scattering center. The values for the search length ranged from 20–200 m (100 m typical), while the search resolution ranged from 0.002–0.2 ns (0.02 ns typical). Alternatively, in the time domain, the scattering centers are separated by a time interval, ΔT_s, which ranged from 0.01–10 ns (0.1 ns typical). To accurately portray the water medium, it is imperative to consider the density of scatterers to be large, which imposes the condition that $\Delta l \ll L$ (or equivalently $\Delta T_s \ll t_d = L/v =$ search time). The sampling time or resolution of the signal is defined by the time increment dt used to divide the 10 ns transmitted pulse into segments. This value is chosen to satisfy the Nyquist criterion [6] (0.01–1 ns, 0.1 ns typical), and therefore makes the simulation fully compatible with various signal processing routines. To produce a realistic simulation, (7) and (8) were augmented to include the relative intensity noise (RIN) of the laser and the noise equivalent power (NEP) of the optical detector. These values were chosen to range from 1–5% (2% typical) for the laser RIN, and 50 pW/Hz$^{1/2}$ for the detector NEP.

The simulation tracks the evolution of the pulse as it propagates from the ocean surface toward the ocean bottom, including the backscatter and target reflection. By updating this information and displaying it on the screen at regular time intervals, an animation is created that provides for good physical insight. The simulation also emulates the receiver with advanced signal processing tools like Fourier transform, averaging, filtering, and heterodyning to determine optimal receiver design. For direct comparison of simulation and laboratory experimental results, the typical values listed above were chosen to represent those used in the laboratory experiment, which are summarized in the next section.

V. Ocean Mass Simulator and Laboratory Experiment

The desire to test experimentally the feasibility of this LIDAR-RADAR detection scheme in a laboratory environment without the cost of actual surveying measurements led to the development of an empirical fiber-based ocean mass simulator (OMS). The main requirements for an ocean mass simulator are that it be a simple, inexpensive, laboratory-based instrument with similar attenuation characteristics to water. It is known that plastic optical fiber has low transmission loss [7] and high scattering loss [8] in the blue-green (532 nm). Optical time domain reflectometry studies have demonstrated that the backscatter process in multimode fibers is comparable to water and is characterized by an exponential decay [9]. Modulated optical time domain reflectometry measurements in optical fiber by Uttam *et al.* [10], MacDonald [11], and Nakayama *et al.* [12] have also shown that the continuous backscatter from optical fiber exhibits a low-pass filterlike frequency response, while Fresnel reflections from fiber breaks and bends are independent of frequency. The comparable attributes pertaining to the propagation and scattering of optical rays in ocean water and large multimode fiber led to the design of the OMS using this fiber.

The completed OMS, reported by Mullen *et al.* [13], consists of 100 m of plastic optical fiber wrapped uniformly around a rod. Different water types are simulated by changing the rod diameter, while a reflection corresponding to that from an

underwater object is produced by bending the fiber sharply at a specific point. Similarities of the backscatter signatures of an actual LIDAR and OMS measurement were identified in [13] and provided confidence in the ability of the OMS to validate experimentally the projected clutter suppression of the hybrid detection scheme.

The experimental setup implementing the LIDAR-RADAR sensor configuration and utilizing the OMS is shown in Fig. 4. The optical source is a Q-switched, frequency-doubled Nd:YAG laser. The modulation frequency is 3 GHz, which is substantially above the backscatter noise cutoff frequency (f_c), and provides 30 cycles of the microwave signal within the laser pulse time. The main challenge in this experimentation is the generation of high-power, microwave-modulated blue-green pulses capable of overcoming the large backscatter dynamic range (~60 dB). The best solution was obtained by using the 3 GHz beat frequency produced by the multilongitudinal mode laser that produced microwave-modulated, blue-green pulses with adequate optical power. The main problem with this modulation source is the lack of pulse-to-pulse repeatability.

At point p_d in Fig. 4, the detected hybrid LIDAR-RADAR signal from the OMS, $P_{dLR}(t)$, is split equally into two signal paths and processed independently. In the LIDAR detection mode, the 100 MHz bandwidth logarithmic amplifier effectively filters the microwave component of the signal, $P_{dR}(t)$, while the LIDAR signal component, $P_{dL}(t)$, is recovered, digitized, and displayed. At the microwave receiver, the low frequency part of the signal, $P_{dL}(t)$, is filtered out by the 500 MHz bandpass filter centered at $f_m = 3$ GHz. Although earlier calculations have shown that implementing a narrower filter is more desirable, the use of a broad bandwidth matched receiver is presently required because of the drift of the modulation source. After passing through the filter, the microwave envelope is amplified, detected, and analyzed. This experimental procedure provides for simultaneous measurement and evaluation of the LIDAR and microwave signal returns.

In the next section, the laboratory experimental results obtained with the setup in Fig. 4 are compared directly with those obtained with the computer simulation. The program incorporated values typical of experimental conditions. As the next section shows, the comparison of simulation and experimental results verifies theoretical predictions and validates the computer model for predicting future improvements achieved with more sophisticated modulation and detection schemes.

VI. Results

The computer simulation and laboratory experimental results of LIDAR and microwave RADAR signal returns of a 10 nsec modulated pulse are summarized in Figs. 5 and 6. In particular, Fig. 5 depicts returns with no target and accents the clutter reduction capacity of the hybrid approach. The target contrast enhancement achieved with the hybrid detection scheme is shown in Fig. 6. Plot 1 in Fig 5(a) represents the computer simulated clutter in a LIDAR return, $S_L(t)$. It is proportional to the received photon intensity, which decreases with return time (or depth of reflection), and

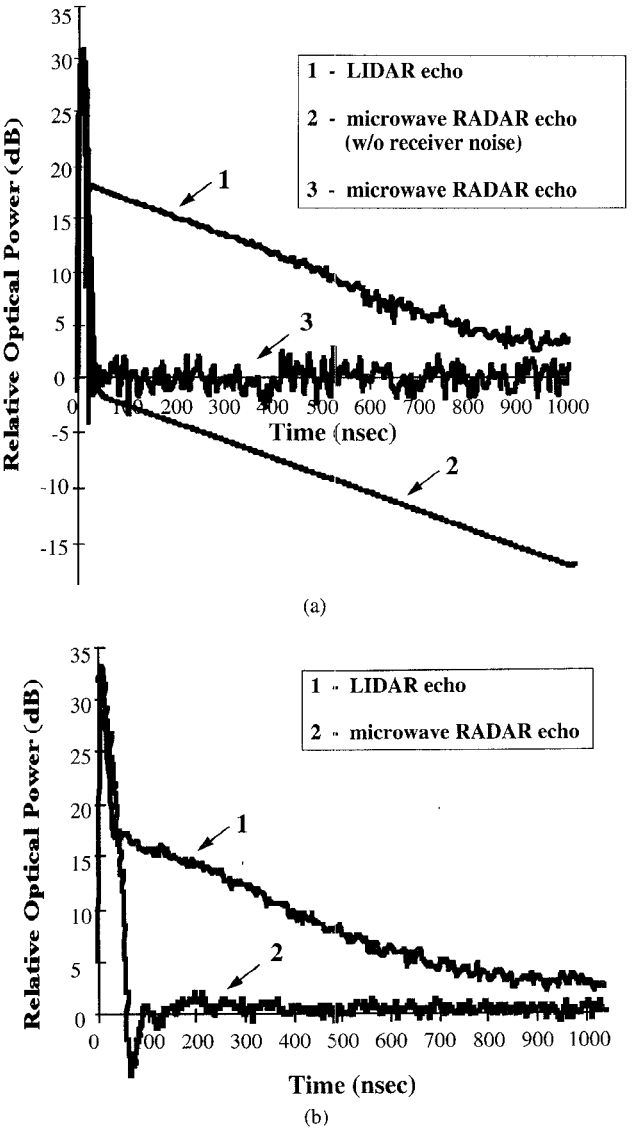

Fig. 5. (a) Computer simulation and (b) experimental LIDAR and RADAR return signals with no underwater target echo present. The suppression of backscatter clutter by 20 dB is shown in (a) for an ideal microwave receiver.

therefore exhibits a characteristic exponential decay. Plot 2 represents the microwave return signal, $S_M(t)$, as recorded by a noise-free ideal receiver. The effect of the 500 MHz filter at 3 GHz is to reduce the photon-dependent clutter level by 20 dB, as predicted. Upon the addition of realistic receiver characteristics to the simulation, the system noise, which is independent of the return signal, exceeds the reduced clutter level shown in plot 3. The corresponding experimental results in Fig. 5(b) are in excellent agreement with the computer simulations, and thus they validate the analytic considerations. It must be emphasized that the implementation of a narrower matched filter (i.e., 3 MHz) would attenuate the clutter level by an additional 20 dB and decrease the microwave receiver noise significantly. This improvement is however contingent on the development of a better modulated transmitter.

The clutter reduction leads directly to enhanced detection sensitivity, as shown in Fig. 6(a) and (b). The graph in

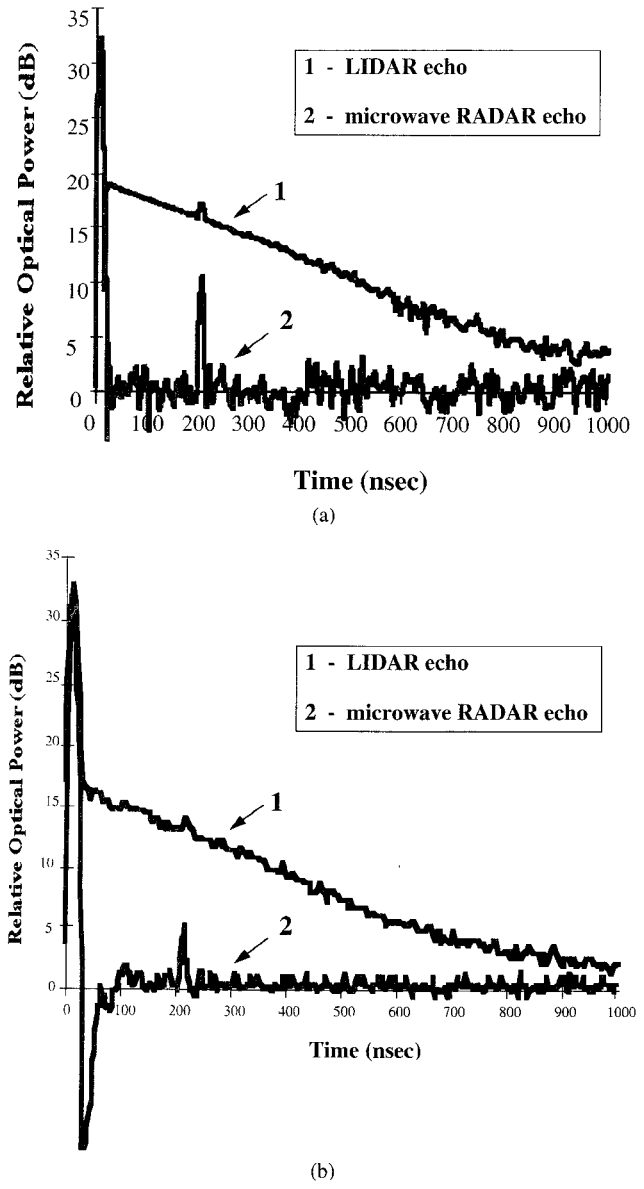

Fig. 6. (a) Computer simulation and (b) experimental LIDAR and RADAR return signals with a reflection from an underwater object. The suppression of backscatter clutter in the RADAR return improves the contrast of the submerged target.

Fig. 6(a) depicts the LIDAR and RADAR simulated echoes with inclusion of a shallow underwater target. The target contrast enhancement is evident by the comparison of the two returns, which are also in good conformity with the experimental results in Fig. 6(b). The target detection sensitivity is now limited by system noise, which can be reduced by transmitter and receiver optimization.

Thus, we see that the main difference between the LIDAR and microwave RADAR returns is the backscatter clutter level. Since the clutter is proportional to the number of photons in LIDAR measurements, there is no incentive to increase the transmitted laser power. However, in the hybrid detection scheme the noise is independent of the photon intensity, and, therefore, one can use shorter pulses with high peak power to improve the signal to noise and spatial resolution of underwater targets.

VII. Conclusion and Future Considerations

Currently, the fastest and most efficient technique for shallow underwater surveying is airborne LIDAR. However, the continuous backscatter of light from water gives rise to clutter, which limits the contrast of near-surface underwater target reflections and, therefore, decreases the detection sensitivity of LIDAR. In this paper, a novel hybrid LIDAR-RADAR detection scheme was introduced. This new approach, which combines the desirable features of microwave RADAR and LIDAR, is designed to improve the detection sensitivity of underwater objects. The viability of this new approach was demonstrated through proof-of-concept experimentation which achieved a 17 dB reduction in near-surface clutter. Computer simulations predict a potential for more significant reductions by improving the hybrid transmitter and receiver.

The accomplishments of the hybrid LIDAR-RADAR system described above led to the desire to plan for a full-scale realization of the laboratory experiment in the actual ocean environment to verify the clutter reduction and investigate dispersion effects. Present efforts include the development of a more reproducible and efficient method for the modulation of a high-power, blue-green optical pulse. The receiver configuration is being optimized with inclusion of sophisticated RADAR signal processing techniques such as matched filter or heterodyning. The refined hybrid LIDAR-RADAR detection scheme is expected to produce improved laboratory experimental results and to further demonstrate the capability of the new system to enhance the detection of shallow underwater objects.

References

[1] G. C. Guenther, "Airborne laser hydrography—System design and performance factors," NOAA Professional Paper Series, Library of Congress Catalog number 85-600602, Mar. 1985.

[2] M. F. Penny, R. H. Abbot, D. M. Phillips, B. Billard, D. Rees, D. W. Faulkner, D. G. Cartwright, B. Woodcock, G. J. Perry, P. J. Wilsen, T. R. Adams, and J. Richards, "Airborne laser hydrography in Australia," *Appl. Opt.*, vol. 25, no. 13, July 1986.

[3] M. I. Skolnik, *Introduction to Radar Systems.* New York: McGraw-Hill, 1962.

[4] B. Billard, R. Abbot, and M. Penny, "Airborne estimation of sea turbidity parameters from the WRELADS laser airborne depth sounder," *Appl. Opt.*, vol 25, no. 13, July 1986.

[5] N. G. Jerlov, *Optical Oceanography.* Amsterdam: Elsevier, vol. 5 1968.

[6] A. Oppenheim and A. S. Willsky, *Signals and Systems.* New Jersey: Prentice-Hall, 1983.

[7] T. Kaino, M. Fujiki, S. Oikawa, and S. Nara, "Low-loss plastic optical fibers," *Appl. Opt.*, vol. 20, no. 17, Sept. 1981.

[8] T. Yamashita, S. Shichijvo, T. Takemura, and K. Matsushige, "Light scattering measurement in PMMA optical fibers," *Japan. J Appl. Phys.*, vol. 26, no. 11, pp L1797–L1799, Nov. 1987.

[9] M. K. Barnoski and S. M. Jensen, "Fiber waveguides: A novel technique for investigating attenuation characteristics," *Appl. Opt.*, vol 15, no. 9, pp. 2112–2115, Sept. 1976.

[10] D. Uttam and B. Culshaw, "Precision time domain reflectometry in optical fiber systems using a frequency modulated continuous wave ranging technique," *J. Lightwave Technol.*, vol. LT-3, no. 5, pp. 971–977, Oct. 1985.

[11] R. I. MacDonald, "Frequency domain optical reflectometer," *Appl. Opt.*, vol. 20, no. 10, pp. 1840–1844, May 1981.

[12] J. Nakayama, K. Iizuka, and J. Nielsen, "Optical fiber fault locator by the step frequency method," *Appl. Opt.*, vol. 26, no. 3, pp. 440–443, Feb. 1987.

[13] L. Mullen, P. R. Herczfeld, and V. M. Contarino, "Analytical and experimental evaluation of an optical fiber ocean mass simulator," *IEEE Microwave and Guided Wave Lett.*, vol. 4, no. 1, pp. 17–19, Jan. 1994

Linda Jeanne Mullen was born in Cherry Hill, NJ, in 1970. She received the B.S. degree in electrical engineering at Trenton State College in Trenton, NJ, in 1992. She received the M.S. degree in electrical engineering at Drexel University in Philadelphia, PA, in 1993.

She is presently a doctoral candidate at Drexel University and is working on a project at the Center for Microwave-Lightwave Engineering at Drexel for the Naval Air Warfare Center in Warminster, PA, for improvements in underwater LIDAR technology. Her research interests include the application of microwave technology to optical modulation and detection in underwater laser radar system design.

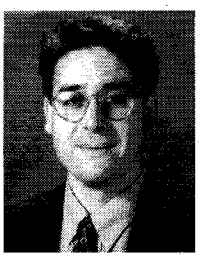

Amarildo J. C. Vieira was born on December 24, 1963, in Sáo Paulo, Brazil. He received the B.S. and M.S. degrees in electrical engineering from Escola de Engenharia de Sáo Carlos, Universidade de Sáo Paulo, Brazil, in 1987 and 1992, respectively.

During the period 1988–1989 he joined NEC Brazil S.A., to work with microwave digital radio systems. He is currently pursuing his Ph.D. degree in electrical engineering at Drexel University, Center for Microwave-Lightwave Engineering, Philadelphia, working in conjunction with the Naval Air Warfare Center, Warminster, both in Pennsylvania. His research interests involve optical sensors and microwave optical modulation for Lidar systems. He is supported by the Council of Research and Development (CNPq), RHAE project, of the Brazilian Government.

Peter R. Herczfeld (S'66–M'67–SM'89–F'91), for a photograph and biography, see this issue, p. 2181.

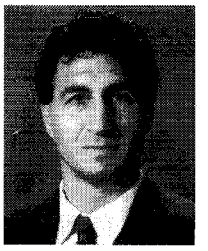

Vincent Michael Contarino was born in Allentown, PA, in 1952. He received the B.S. degree in physics from Lafayette College in Easton, PA, in 1975. In 1983, he received the M.S. degree in engineering and computer science from Pennsylvania State University. The Ph.D. degree in electrophysics was conferred by Drexel University in Philadelphia, PA, in 1989.

Since 1977, he has been employed by the Naval Air Warfare Center in Warminster, PA (formerly the Naval Air Development Center). His background has been in the development of pulsed blue-green air to underwater laser radar systems. Research areas include optical–microwave interaction, microwave optical modulation, and LIDAR component development.

Dr. Contarino received the 16th European Microwave prize in 1986 for his Ph.D. work at Drexel University.